CrossMark

Can the Tibetan Plateau snow cover influence the interannual variations of Eurasian heat wave frequency?

Zhiwei Wu[1] · Peng Zhang[1] · Hua Chen[1] · Yun Li[2]

Abstract The Eurasian continent has experienced significant year-to-year variations of summer heat waves during the past decades. Several possible factors, such as ocean temperature, soil moisture, and changes in land use and greenhouse gases, have been identified in previous studies, but the mechanisms are still unclear. In this study, it is found that the Tibetan Plateau snow cover (TPSC) is closely linked to the interannual variations of summer heat waves over Eurasia. The TPSC variability explains more than 30 % of the total variances of heat wave variability in the southern Europe and northeastern Asia (SENA) region. A set of numerical experiments reveal that the reduced TPSC may induce a distinct teleconnection pattern across the Eurasian continent, with two anomalous high pressure centers in the upper troposphere over the SENA region, which may lead to a reduction of the cloud formation near the surface. The less cloud cover tends to increase the net shortwave radiation and favor a stronger surface sensible heat flux in the dry surface condition over the SENA region, resulting in a deeper, warmer and drier atmospheric boundary layer that would further inhibit the local cloud formation. Such a positive land–atmosphere feedback may dry the surface even further, heat the near-surface atmosphere and thereby intensify the local heat waves. The above dynamical processes also operate on interdecadal time scales. Given the reduction of the TPSC could become more pronounced with increasing levels of greenhouse gases in a warming climate, we infer that the TPSC may play an increasingly important role in shaping the summer heat waves over the SENA region in next decades.

1 Introduction

During the recent decade, many regions in Eurasia have experienced frequent heat wave activities which have disastrous impacts on the society (Alexander 2010; Trenberth et al. 2007). For instance, over 25,000 deaths were related to the 2003 heat wave in Europe (D'Ippoliti et al. 2010). The heat-related mortality exceeded 15,000 across the northeastern Europe and Russia in the summer of 2010, when 33 consecutive days with maximum temperatures exceeding 30 °C were recorded (Barriopedro et al. 2011). Northern China has also undergone frequent heat wave activities within the past decades (Zhai et al. 1999; Fu 2003; Wang and Ding 2006; Ding et al. 2007; Wu et al. 2012a). More than half a billion people are under the threat of drinking water shortages. Therefore, it is of great importance to understand the origins of the Eurasian heat wave variability.

A number of processes, such as ocean temperature, soil moisture, and changes in land use and greenhouse gases, have been identified as possible contributors in these temperature extreme events. Sutton and Hodson (2005) suggested that basin-scale changes in the Atlantic Ocean acted as an important driver of multi-decadal variations in the summertime climate of Europe. Using a regional climate model, Fischer et al. (2007) noted that soil moisture

✉ Zhiwei Wu
zhiweiwu@nuist.edu.cn

[1] Earth System Modeling Center (ESMC) and Key Laboratory of Meteorological Disaster of Ministry of Education, Nanjing University of Information Science and Technology, Nanjing 210044, Jiangsu, China

[2] CSIRO Digital Productivity Flagship, Leeuwin Centre, Floreat, WA 6014, Australia

in spring was an important parameter for the evolution of European heat waves and the lack of soil moisture strongly reduced latent cooling and thereby amplified the surface temperature anomalies. Fu (2003) pointed out that the human-induced land cover changes result in significant changes of surface dynamic parameters, such as albedo, surface roughness, leaf area index and fractional vegetation coverage, etc., which might impact the Eurasian climate, particularly northern China. Meehl and Tebaldi (2004) found that the present-day heat waves over Europe coincided with a specific atmospheric circulation pattern that was intensified by ongoing increases of greenhouse gases. Although these factors have been identified as possible causes, the mechanisms of Eurasian heat wave variability are still unclear.

Sitting at an average height of around 4000 m above sea level, the Tibetan Plateau (TP) protrudes into the middle of the troposphere, where most weather events originate (Qiu 2014). As the biggest and highest plateau in the world, it disturbs this part of the atmosphere like no other structure on Earth, but many of the details are a mystery. The TP snow cover (TPSC) is a crucial index to measure the thermal condition of TP. With the high altitude of TP, the TPSC can persist into high altitudes through the warm seasons (Pu et al. 2007), making it a potential source of predictability for summer climate (e.g., Wu et al. 2012a, b). Can the TPSC influence the variability of Eurasian heat waves? In this study, we attempt to answer this question.

In contrast to quite a few previous studies on the climate impacts of the Eurasian snow cover (Barnett et al. 1988; Gong et al. 2002, 2003, 2004; Fletcher et al. 2009; Sobolowski et al. 2010; and many others), the amount of research on the TPSC has been relatively small. This is partially due to the reason that the TPSC was usually considered to part of the Eurasian snow cover (Clark and Serreze 2000), as well as the lack of enough observations over TP, particularly over western TP (Wang et al. 2008). As a matter of fact, the climate impact of the TPSC is distinguished from that of the Eurasian snow cover. For instance, the TP warming associated with the glacial retreat could induce two distinct Rossby wave trains, which could modulate the variations of Meiyu–Baiu–Changma rain belt (Wang et al. 2008). The anomalous autumn and winter TPSC might trigger a distinct teleconnection pattern similar to the Pacific-North American (PNA) pattern and influence the North American winter climate (Lin and Wu 2011). The anomalous TPSC was found to be responsible for the extreme climate conditions in most of the Northern Hemisphere in the winter of 2009–2010 (Lin and Wu 2012a). These unveiled dynamical processes are distinct from those associated with the Eurasian snow cover, the Siberian snow cover in particular (Gong et al. 2002, 2003, 2004).

In this study, we attempt to answer two questions: (1) Can the TPSC anomalies affect the interannual variability of the Eurasian heat waves during boreal summer? (2) To what extent and how can the TPSC anomalies influence the variability of the Eurasian heat waves? The rest of the paper is structured as follows. Section 2 describes the data, model and methodology used in this study. Section 3 presents the observed relationship between the TPSC and Eurasian heat wave activities. In Sect. 4, numerical experiments are performed with a simple general circulation model (SGCM) and the possible physical processes are discussed in Sect. 5. Section 6 summarizes major findings and proposes some outstanding issues.

2 Data, model and methodology

The datasets used in this work include: (1) 1967–2014 monthly snow cover from the Global Snow Lab (Rutgers University) (http://climate.rutgers.edu/snowcover), which were obtained using polar sterographic projection of Northern Hemisphere with central meridian −80 and each monthly matrix having 89 × 89 grid (Robinson et al. 1993; Robinson and Frei 2000); (2) the Global Historical Climatology Network—daily (GHCND) maximum surface air temperature from the United Kingdom's Hadley Center for the period 1967–2014 (Caesar et al. 2006); (3) the monthly mean atmospheric fields, taken from the National Centers for Environmental Prediction–National Center for Atmospheric Research (NCEP–NCAR) Twentieth Century Re-Analysis Project for the period 1967–2012 (Whitaker et al. 2004; Compo et al. 2006, 2011).

The numerical experiments are based on the SGCM (Hall 2000). The resolution used here is triangular 31 (T31), with 10 equally spaced sigma levels (Wu et al. 2009). The SGCM uses a time-averaged forcing calculated empirically from observational daily data. As shown in Hall (2000), this model is able to reproduce remarkably realistic stationary planetary waves and broad climatological characteristics of the transients. The advantage of this model is that dynamical mechanisms are easily isolated. The limitation is that the physical parameterizations are replaced by empirically derived terms, leading to absence of some potentially important physical feedback mechanisms from our analysis. In this study, the SGCM is used to examine whether the anomalous TPSC can induce a southern Europe -northeastern Asia (SENA) teleconnection pattern or not (see Sect. 3), and does not involve whether the SENA pattern can affect the TPSC variability. Therefore, the limitation of this model does not influence the conclusion of this work.

Following Fischer and Schär (2010), a heat wave in this paper refers to a spell of at least six consecutive days with

Fig. 1 **a** Long-term mean (%) (*contours*) and standard deviations (%) (*color shadings*) of the Tibetan Plateau (TP) snow cover (TPSC) during boreal summer (June–July–August, JJA) for the period 1967–2014. The areas included by the purple curves are 3000 m above sea level. **b** The normalized TPSC index (TPSI) time series (*black curve*) defined by the TPSC averaged in the *purple-boxed area* (70°–80°E, 31°–41°N) in **a** (Wu et al. 2012b). The *red curve* indicates the detrended component of the TPSI, hereafter TPSI(DT). The *dashed lines* denote 1/−1 standard deviation of the normalized TPSI
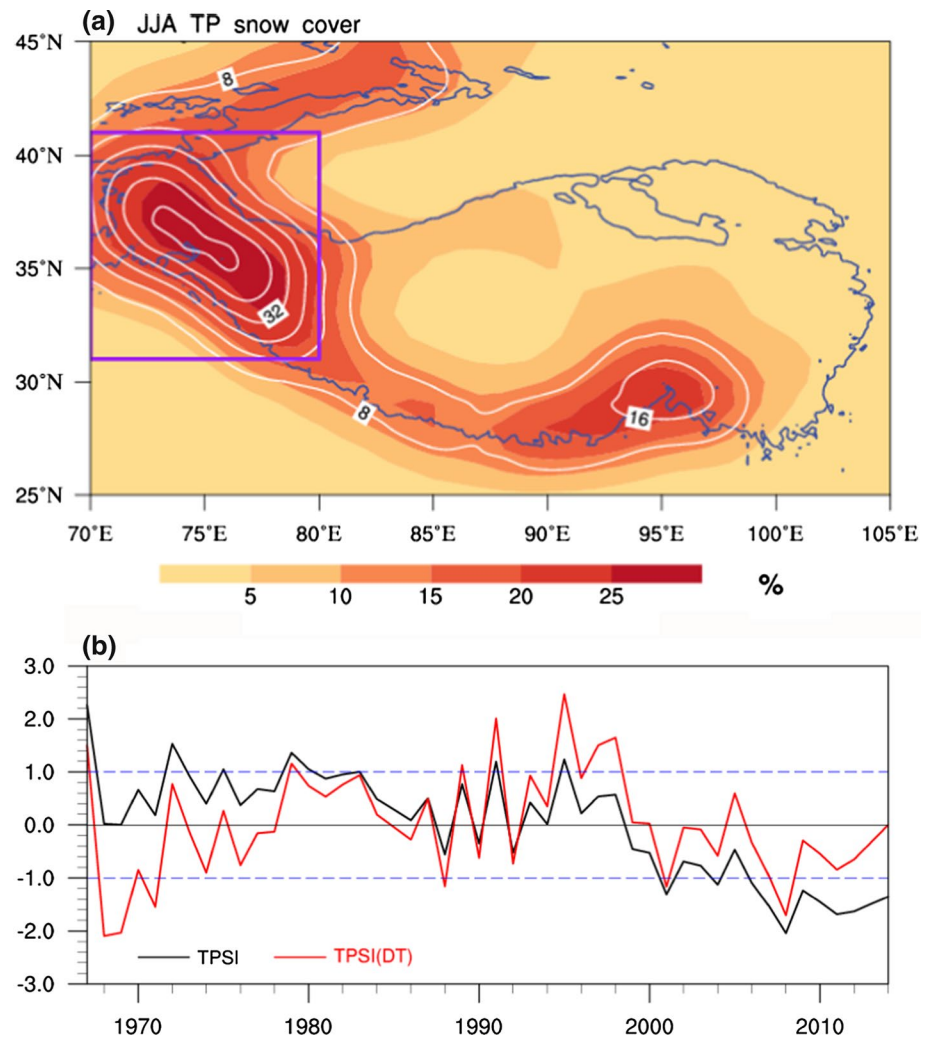
daily maximum temperature exceeding 90th percentile of the period (1967–2014). To account for the seasonal cycle, the 90th percentile is calculated for each calendar day and at each grid point, using a centered 15-day-long time window. With a moving window, the temporal dependence of heat waves is accounted for and the sample size is reasonable to calculate a realistic percentile value (Perkins and Alexander 2013). The heat wave frequency (HWF) is defined as the number of days satisfying the heat wave criterion in a summer. To derive the leading modes of the HWF, we perform an Empirical Orthogonal Function (EOF) analysis by using a covariance matrix.

In this study, a TPSC index (TPSI) is used to quantify the TPSC variability and is defined as the snow cover anomaly averaged within the TP domain (70°–80°E, 31°–41°N) where the summer climatology center and the maximum year-to-year variability are located (purple box in Fig. 1a). Wu et al. (2012b) found that the snow cover anomaly in the above TP domain persisted from spring through summer, serving as a stable precursor for seasonal prediction. The TPSI provides an optimal representation of the spatial–temporal variability of the TPSC during boreal summer.

3 TPSC and the Eurasian HWF

Figure 1a presents the climatology and standard deviation of the TPSC in the boreal summer for the period 1967–2014. The major snow cover areas are primarily located in the large mountain ridges, namely, western and southern TP (contours in Fig. 1a), which is consistent with the Moderate Resolution Imaging Spectroradiometer (MODIS) on the Terra spacecraft (Pu et al. 2007). These snow cover areas also exhibit a strong year-to-year variability with relatively high standard deviation values (color shadings in Fig. 1a). Such notable changes in snow cover may lead to significant variation of the atmospheric diabatic heating in the middle troposphere (Zhong et al. 2013).

Fig. 2 **a** Time series of the principal component (PC) (*blue* and *red bars*) and **b** spatial pattern (*color shadings*; in unit of days) of the first EOF mode (EOF1) of heat wave frequency (HWF) over the Eurasian continent for the period 1967–2014. **c** The HWF fractional variances explained by the TPSC (color shadings; in unit of %). The *black curve* in Fig. 2a represents the TPSI time series defined in Fig. 1b. For comparison purpose, the sign of the TPSI time series has been reversed. The two *purple-boxed areas* in Fig. 2c denote the southern Europe (10°–25°E, 40°–50°N) and northeastern Asia (100°–140°E, 45°–60°N) (SENA) region
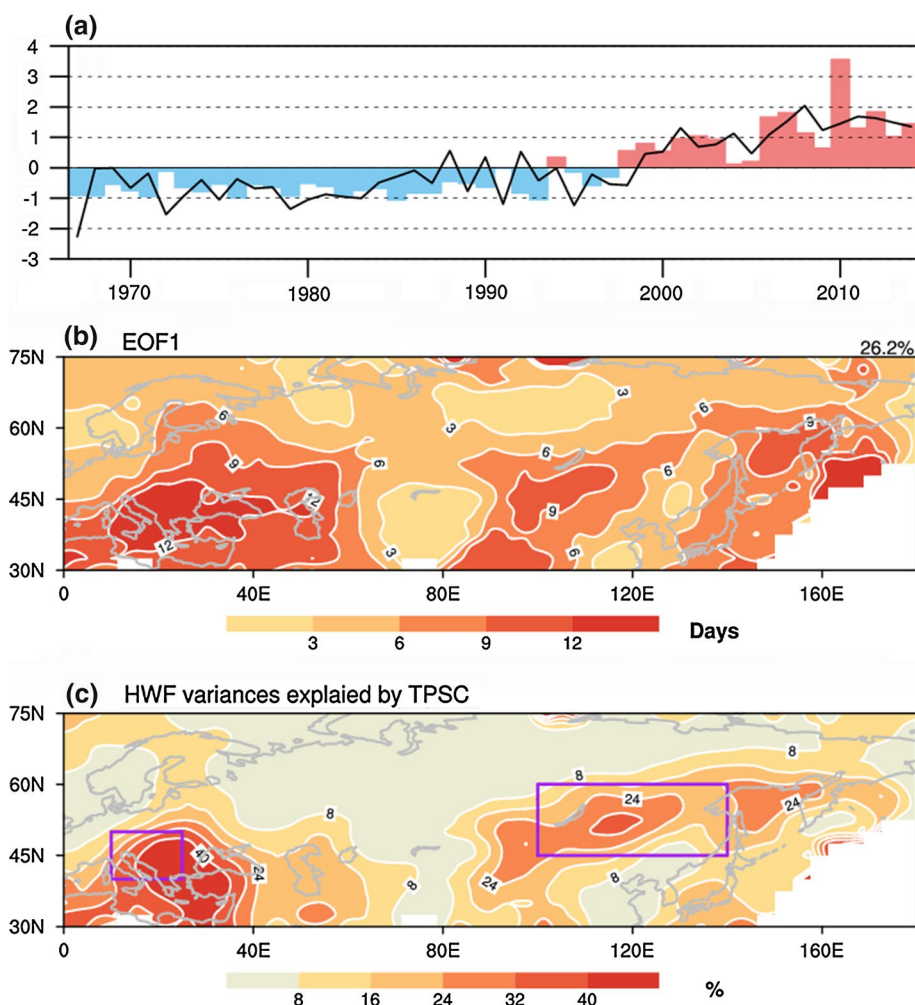
To quantitatively measure the year-to-year variations of the summer TPSC, the snow cover index TPSI is used following Wu et al. (2012b), which is defined as the snow cover anomaly averaged within the TP domain (70°–80°E, 31°–41°N). Figure 1b shows the temporal evolution of the normalized TPSI for the past 48 summers (1967–2014). A prominent feature is that the TPSC exhibits a pronounced decreasing trend with slope −0.06 standard unit/year, significant at the 99 % confidence level. Meanwhile, the observed surface air temperature at 90 gauge stations at TP shows a warming trend though most of them are located in the eastern TP (fig. 1d in Wang et al. 2008).

Corresponding to the pronounced reduction in summer TPSC, the HWF over the Eurasian continent primarily exhibits an increasing trend (Fig. 2). For instance, the first principal component (PC1) is dominated by an increasing trend superimposed on modest interannual variations (Fig. 2a). The spatial pattern of the first mode (EOF1), which accounts for 26.2 % of the total variance, is characterized by a single-sign pattern with a maximum center in southern Europe (Fig. 2b). According to the criterion of

North et al. (1982), this mode is statistically significantly distinguished from other modes. It mainly reflects the increase of HWF over Eurasia.

The TPSI (black curve in Fig. 2a) basically exhibits a coherent variation with PC1. The correlation coefficient between PC1 and the TPSI is −0.74 for the raw time series and −0.3 for the detrended components, both exceeding the 95 % confidence level based on the Student's-*t* test. The TPSC is also significantly related to the heat waves in the SENA region (as shown by two boxes in Fig. 2c). It explains more than 30 % of the total variance of the local HWF, particularly over southern Europe where the TPSC can account for more than 40 % of the local HWF variance. However, the statistical linkage between the TPSC and Eurasian heat waves does not warrant any causal relationship. Then, can the TPSC influence the Eurasian HWF?

Before answering the above question, we need to clarify the dynamic structures of the large-scale circulation associated with the TPSC anomalies. Considering that the TPSI is dominated by an increasing trend, the following analyses are done using the detrended component of TPSI, namely,

Fig. 3 JJA geopotential height anomalies regressed against the TPSI(DT) (*contours*; in unit of gpm) at **a** 200 and **b** 500 hPa. Geopotential height(DT) denotes its detrended component. The contour interval is 2 gpm. An SENA index is defined as the difference of 200 hPa geopotential height between the *box with positive values* (50°–90°E, 60°–75°N) and the *two boxes with negative values* [(10°–25°E, 25°–45°N) and (100°–130°E, 50°–60°N)]. The shaded areas exceed the 90 % confidence level
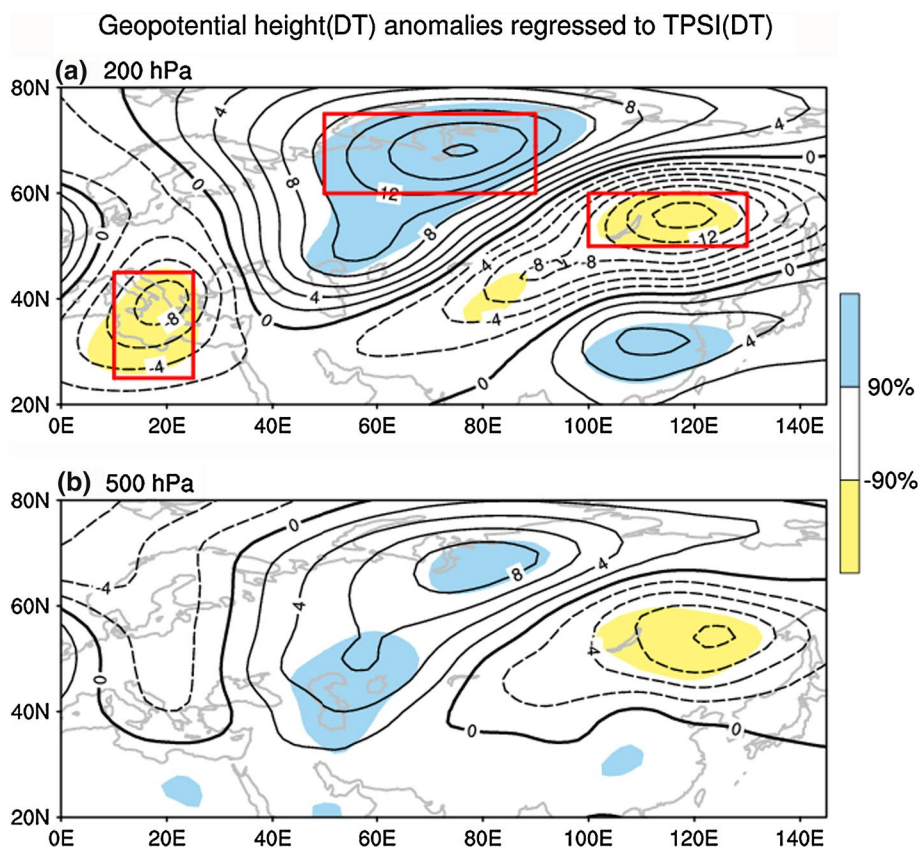
TPSI(DT) hereafter. The linear trends of the circulation fields, such as geo-potential height at 200 and 500 hPa (Z200 and Z500), and low cloud cover (LCC) are also removed. Moreover, since the TPSI exhibits some fractions of decadal-interdecadal variations (Fig. 1b), we calculated its effective freedom degree (Trenberth 1984; Bretherton et al. 1999), which is around 42–43.

Figure 3a displays Z200 anomalies regressed against the TPSI(DT). An evident feature is a Eurasian wave train in the mid-and-high latitudes north of 30°N, prevailing over the region from the North Atlantic to the Okhotsk Sea. Associated with this wave-train pattern, two negative Z200 anomaly centers are located over the SENA region and one positive center over the western Siberia. Z500 exhibits a similar anomalous pattern with Z200 (Fig. 3b). This barotropic structure reflects that this wave-train pattern might be an extratropical response to a remote forcing (e.g., Lin and Wu 2012b).

To further check whether the relationship between the TPSI(DT) and Z200 is robust or not, a field significance test proposed by Livezey and Chen (1983) based on Monte Carlo simulations are employed to evaluate the field significance of correlation patterns in Fig. 3a. The TPSI(DT) time series are replaced with a random time series sampled from a Gaussian distribution N(0, 1). Then, correlations between these random time series and the Eurasian Z200

are obtained at every grid point and tested for significance. This experiment is completed a total of 1000 times with different random inputs and all results are presented in Fig. 4. The shadings in Fig. 3a represent 23.5 % of the total area consisting of 2263 grid points. Because at least 10 % of the trials have greater than 17.0 % of their area statistically significant at the 90 % confidence level, the hypothesis that the result shown in Fig. 3a is a chance occurrence can be rejected at the 90 % confidence level (Fig. 4). That is to say, they are significant fields at the 90 % confidence level.

In this study, the wave-train pattern shown in Fig. 3a is labeled as the SENA teleconnection. It is not only different from the circum-global teleconnection (CGT) wave-train pattern excited by the Indian summer monsoon (Ding and Wang 2005; Lin 2009), but also different from the subpolar teleconnection pattern excited by the tri-pole sea surface temperature anomaly in the North Atlantic (Wu et al. 2009, 2012c). To quantitatively depict this pattern, we propose an SENA index as the difference of Z200 between the box with positive values and the two boxes with negative values as shown by Fig. 3a. It should be pointed out that the above speculation on the anomalous TPSC and the SENA teleconnection pattern is solely based on statistical analysis, which cannot guarantee causal relationship.
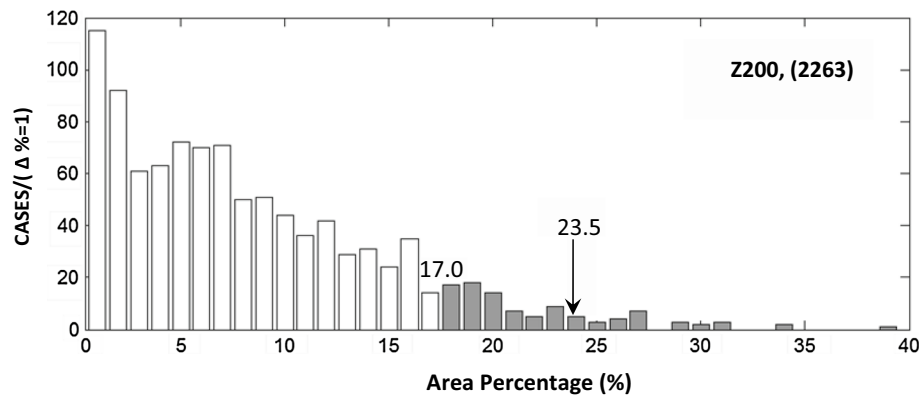
Fig. 4 Histograms of percent of area with correlations of JJA 200 hPa geopotential height (Z200) and Gaussian noise statistically significant at the 90 % confidence level in 1000 Monte Carlo trials. The abscissa is percent of area while the ordinate is number of cases for each 1 % interval. The 10 % tail is schematically shown by shading the 100 of 1000 largest percents. The results for correlations with the TPSI(DT) in Fig. 3a are shown by *vertical arrows*

Fig. 5 a Vertically averaged anomalous heating rate for the TPSC forcing run (*blue contours*). The contour interval is 0.5 K day^{-1}. **b** Responses of JJA 200 hPa geopotential height (Z200) against the anomalous TPSC forcing in the Simplified General Circulation Model (SGCM) (excessive minus reduced TPSC). The contour interval is 5 gpm. The anomalies are greater than 20 gpm in the *green areas*, and less than −20 gpm in the *blue areas*. The *three red boxes* are the same as those in Fig. 3, which are used to define the SENA teleconnection index
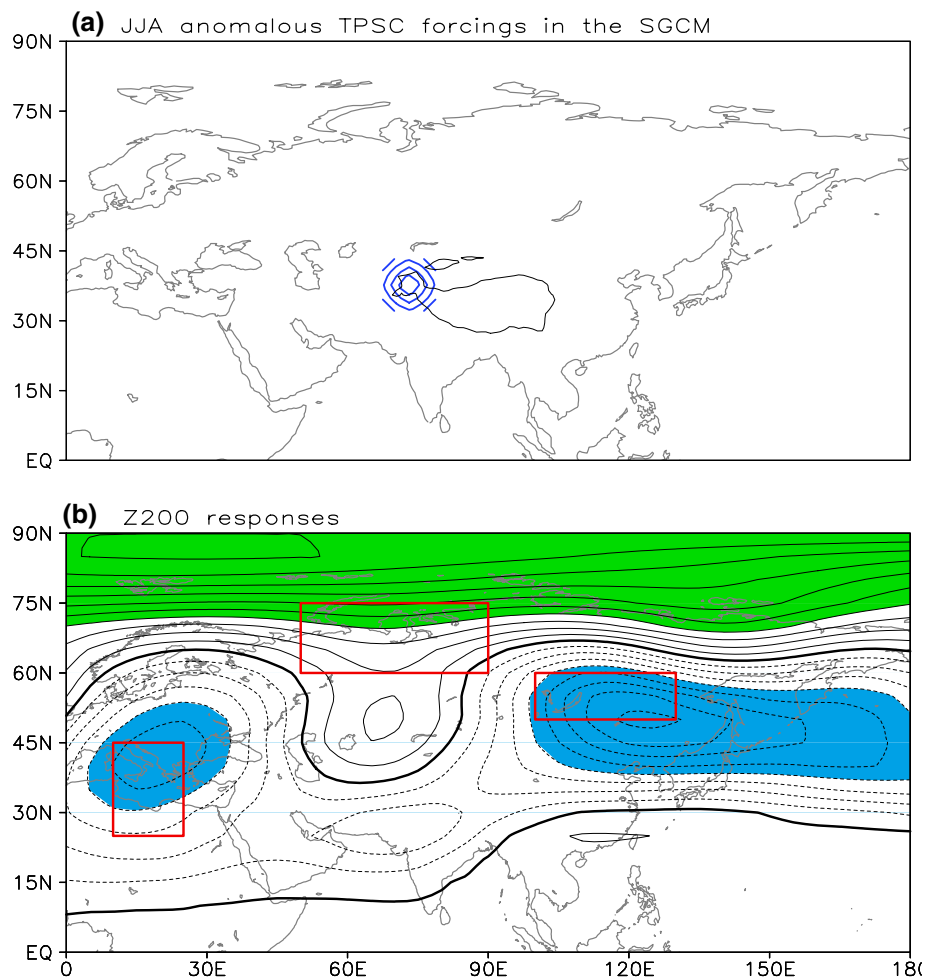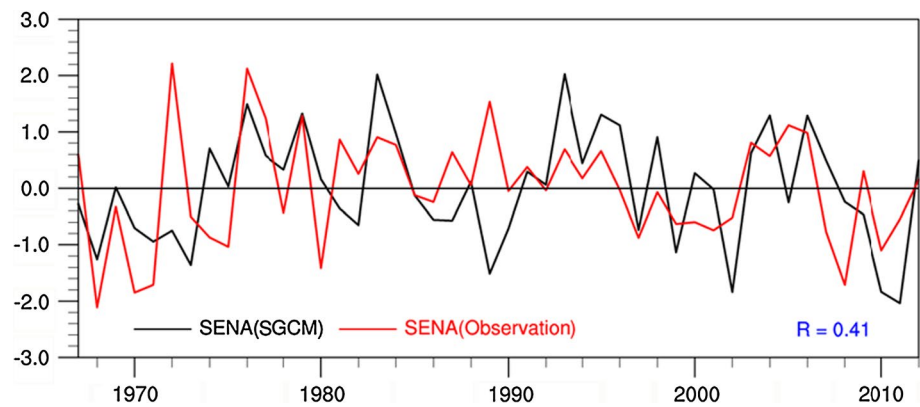
Fig. 6 Time series of the observed (*red curve*) and simulated (*black curve*) SENA index during the latest 46 summers (1967–2012). The correlation coefficient (R) between them is 0.41, exceeding the 95 % confidence level based on the Student's-*t* test

4 Numerical experiments

To elucidate the effects of an anomalous TPSC forcing on the SENA teleconnection pattern, first we perform the reduced and excessive TPSC experiments with the SGCM. To mimic the diabatic heating of the reduced TPSC, we impose a warming anomaly centered at 75°E, 35°N which has an elliptical squared cosine distribution in latitude and longitude with a maximum heating near 500 hPa being 2.5 K/day (Fig. 5a). For the excessive TPSC, the sign is reversed. According to the vertical profile of diabatic heating over TP (Luo and Yanai 1984; Zhong et al. 2013), the maximum heating rate over TP during summer can reach 4–5 K/day. In this study, a heating rate of 2.5 K/day is used as a typical value in an idealized experiment. To make the numerical results more robust, the SGCM is integrated for 12 years and the last 10 years' integration is used to derive a reference state. The two perturbation experiments are integrated for 10 years each and a 10-member ensemble (arithmetic) mean is constructed to reduce the uncertainties arising from differing initial conditions.

The model responses of Z200 to the excessive and reduced TPSC forcings are shown in Fig. 5 (excessive minus reduced TPSC). Two negative anomaly centers are induced at upper troposphere, one located over southern Europe and the other over northeastern Asia extending westward to the southeastern Europe. Therefore, the SENA region is largely controlled by higher pressure anomalies in a reduced TPSC summer than in an excessive TPSC summer. This confirms the previous argument that the reduced TPSC forcing may excite high pressure anomalies at the upper troposphere over the SENA region. Note that the simulation has discrepancies in high latitudes (the Arctic in particular), compared with Fig. 3a. It implies that the TPSC anomaly cannot fully explain the circulation variations over the polar region, and that some other factors may dominate the circulations there.

To further verify whether the anomalous TPSC can induce the year-to-year variations of the SENA-like circulation responses, 46-year SGCM experiments are performed with the diabatic heating associated with the variability of the proxy TPSC index during the 1967–2012. To mimic the diabatic heating of the TPSC year-to-year variations, a heating rate of 1 K/day is used as a typical value to denote one standard deviation of the TPSC variability. Figure 6 presents the observed and simulated SENA index time series. Their correlation coefficient reaches 0.41, exceeding the 95 % confidence level based on the Student's-*t* test. This indicates that the intimate connection between the anomalous TPSC and the SENA-like circulation anomalies over Eurasia.

To better understand the dynamical processes that determine the extratropical response to the anomalous TPSC forcing, a linear perturbation model is used on the basis of SGCM, as described in Hall and Derome (2000). The basic state is the model climate of a long summer perpetual nonlinear integration of the SGCM. The model responses of Z200 perturbations from day 3 to 15 to the reduced TPSC forcing are shown in Fig. 7. A positive anomaly is induced at upper troposphere over TP on Day 3, which develops and extends westward towards southern Europe from Day 3 through Day 15. Meanwhile, a high pressure anomaly emerges and develops over northeastern Asia. This numerical experiment also demonstrates that the anomalous TPSC forcing can excite the SENA teleconnection pattern which is similar to the observations.

5 Physical processes

Previous studies suggested that cloud cover near the surface may alter the net shortwave radiation and play critical roles in the heat wave formation in drought conditions (Alexander 2010; Hirschi et al. 2010; Wu et al. 2012a). Figure 8 presents the LCC anomalies regressed against

Fig. 7 Z200 linear responses to the reduced TPSC forcing in the SGCM from Day 3 through Day 15. The interval of the contours is 10 gpm. The anomalies are greater than 20 gpm in the *green areas*, and less than −20 gpm in the *blue areas*
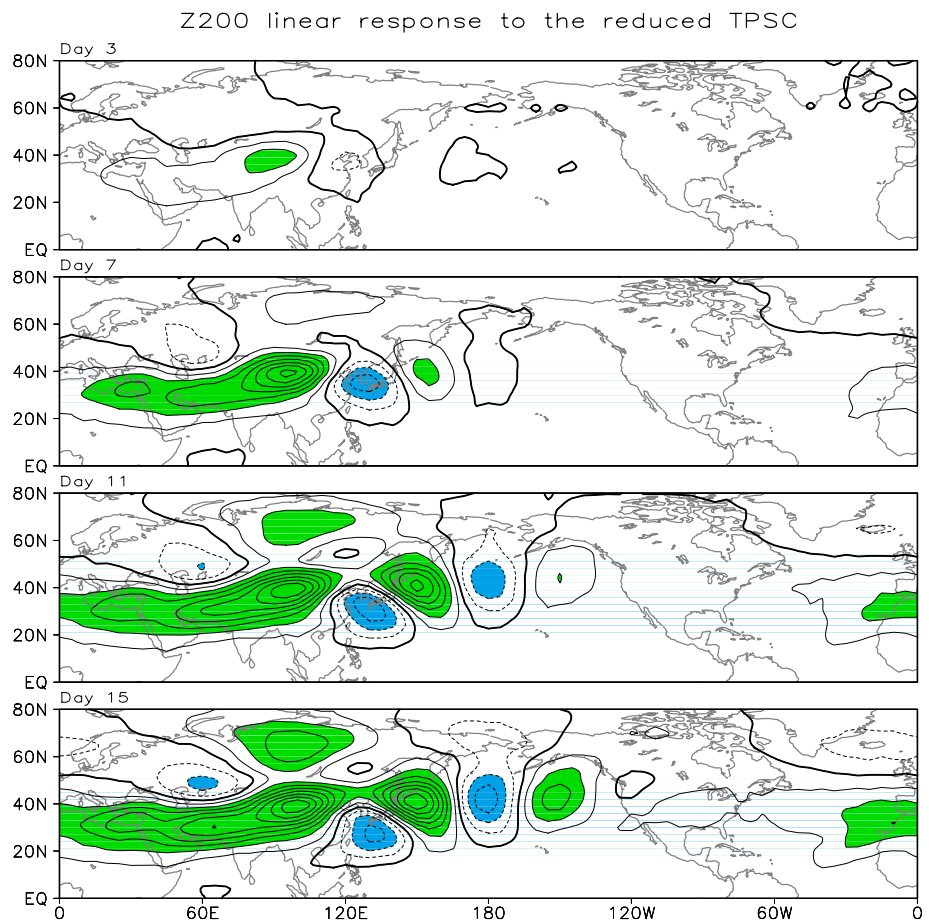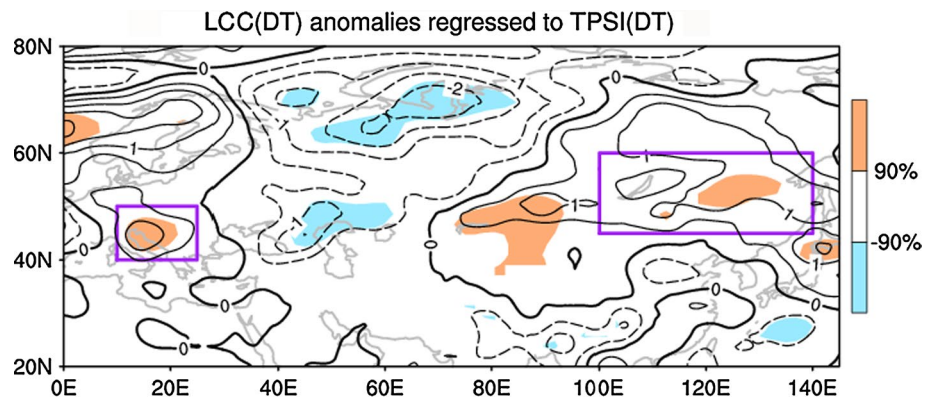

Fig. 8 Same as Fig. 3, but for low cloud cover (LCC) (in unit of %). LCC(DT) denotes the detrended component of LCC. The contour interval is 0.4. The *shaded areas* exceed the 90 % confidence level

the TPSI(DT). Overlapped with the two negative Z200 anomaly centers (shown in Fig. 3), large areas of significant positive LCC anomalies prevail over the SENA region, and vice versa. In light of the intimate linkages among the TPSC, the SENA pattern, LCC and HWF, a hypothesis is proposed as follows: reduced TPSC may induce a negative teleconnection SENA pattern with high pressure anomalies centered over southern Europe and northeastern Asia, respectively. The local upper-troposphere high pressure anomalies associated with divergent flows could reduce the

local LCC. The reduced LCC is related to more net short-wave radiation near surface, thus favoring more heat waves.

To further investigate whether the anomalous TPSC can influence LCC over the SENA region through triggering the SENA teleconnection, the partial-regression approach is used to remove the SENA signal from the LCC (Fig. 9). Compared to Fig. 8, the areas with significant positive coefficients are largely reduced or even vanished over the SENA region, particularly over northeastern Asia. This confirms the previous assumption that the TPSC may

Fig. 9 Same as Fig. 4, except for partial regression with the SENA index signal removed
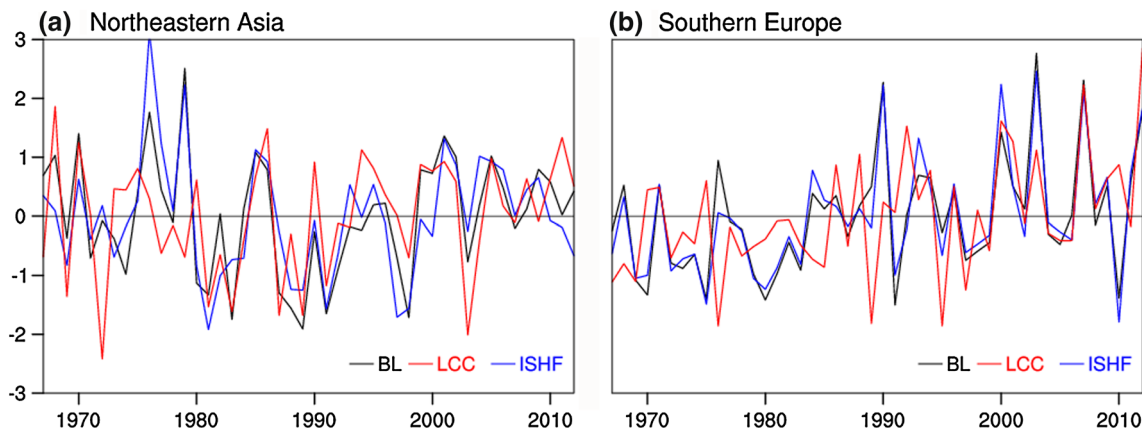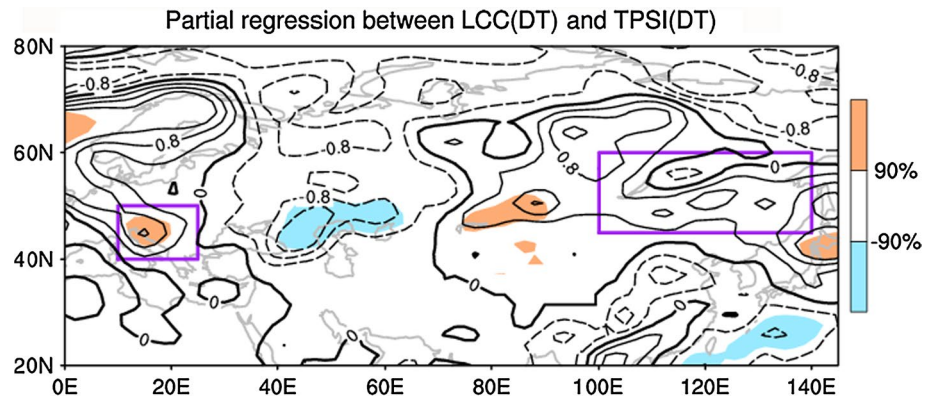

Fig. 10 Time series of the BL, LCC and instantaneous surface sensible heat flux (ISHF) indices for **a** northeastern Asia and **b** southern Europe during the latest 46 summers (1967–2012). The LCC and ISHF indices for northeastern Asia and southern Europe are defined as the averaged LCC and ISHF anomalies in the *two boxes* in Fig. 2c, respectively. The BL index definition can be found in Sect. 5. All these indices have been normalized. For comparison purpose, the signs of the LCC and ISHF indices have been reversed

modulate the local LCC over the SENA region through exciting the SENA teleconnection pattern in the upper troposphere.

Alexander (2010) and Hirschi et al. (2010) proposed a positive land–atmosphere feedback process among heat waves, local LCC, atmospheric boundary layer, and surface sensible heat flux (not shown). Reduced LCC is usually associated with more net shortwave radiation and more surface sensible heat flux, producing a warmer and deeper atmospheric boundary layer that tends to further reduce LCC. Such a positive land–atmosphere feedback favors intensification of extreme heat conditions. However, it is still not clear whether or not the above positive land–atmosphere feedback exists in the SENA region.

To quantify the local atmospheric BL conditions, a BL index is defined as the sum of the normalized BL height and surface air temperature averaged over the southern Europe (10°–25°E, 40°–50°N) and northeastern Asia (100°–140°E, 45°–60°N) as shown by Fig. 2c, respectively. A high BL index corresponds to a warmer and

Table 1 Correlation coefficients among the indices of BL, LCC and ISHF for northeastern Asia

Index	BL	LCC	ISHF
BL	1		
LCC	*0.52*	1	
ISHF	*0.81*	*0.33*	1

The bold italic correlation coefficients exceed 95 % confidence level based on the Student's-*t* test

BL boundary layer, *LCC* low cloud cover, *ISHF* instantaneous surface sensible heat flux

deeper BL, and vice versa. Figure 10 displays the fluctuations of LCC, atmospheric boundary layer (BL), and instantaneous surface sensible heat flux (ISHF) indices for the past 46 summers in southern Europe and northeastern Asia, respectively. An evident feature is the in-phase relationship among them. This result can also be derived from Tables 1 and 2. The BL, LCC and ISHF are significantly

Table 2 Same as Table 1, except for southern Europe

Index	BL	LCC	ISHF
BL	1		
LCC	*0.42*	1	
ISHF	*0.95*	*0.5*	1

correlated with each other in northeastern Asia and southern Europe, respectively. All these indicate that the positive land–atmosphere feedback mentioned above operates in the SENA region.

To summarize, the primary response of the atmosphere to the reduced TPSC is the SENA teleconnection pattern associated with upper-troposphere high pressure anomalies over the SENA region. Such high pressure anomalies trigger the local positive land–atmosphere feedback, which in turn favors more heat waves over the SENA and adjacent regions. For the excessive TPSC, the situation tends to be opposite.

6 Conclusion and discussion

Being the largest and highest plateau in the world, TP has tremendous impact on climate, but many of the details are a mystery (Qiu 2014). Meanwhile, extreme weather and climate events, such as heat waves, have become fervent research foci during the past decade (D'Ippoliti et al. 2010; Barriopedro et al. 2011; Wu et al. 2012d). The origin of the variability of the Eurasian heat waves remains an outstanding issue. In this study, we examined the observed relationship between the TPSC and Eurasian HWF and found that the anomalous TPSC has an intimate linkage with the summer heat waves over Eurasia, particularly over the SENA region. The TPSC variability explained more than 30 % of the local variances of the heat waves. Numerical experiments showed that reduced TPSC could induce a distinct SENA teleconnection pattern across the Eurasian continent, with two anomalous high pressure centers prevailing over the SENA region. Note that the SGCM experiment is an idealized one, due to its simplicity in physics. It cannot provide an accurate quantitative result, but a qualitative one instead.

How could the SENA circulation anomalies influence the Eurasian HWF? The physical processes between the SENA circulation anomalies and HWF can be summarized as follows: The upper-troposphere high pressure anomalies associated with the SENA teleconnection pattern triggered by a reduced TPSC anomaly may inhibit the local LCC; Owing to dry landscapes in the SENA region, the reduced local cloud cover increases the net shortwave radiation, favors a stronger surface sensible heat flux, and produces a deeper,

warmer and drier atmospheric boundary layer that tends to further inhibit the local LCC; Such a positive land–atmosphere feedback may further dry the surface, heat the near-surface atmosphere and in turn intensify the local HWF. The above physical process also operates on interdecadal time scales. Since the TPSC is expected to further decrease with increasing levels of greenhouse gases in the atmosphere in
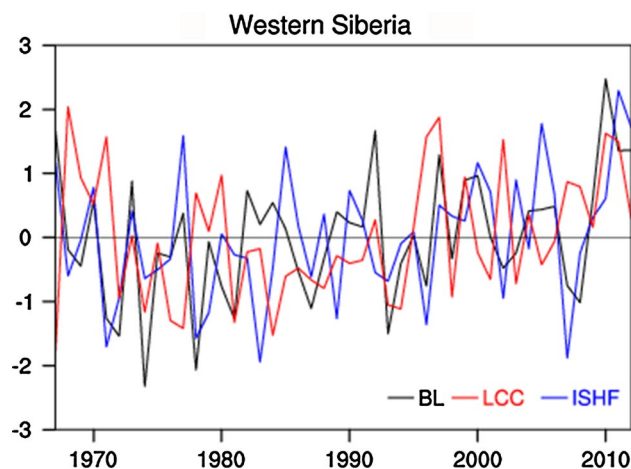

Fig. 11 Same as Fig. 10, except for western Siberia. The indices are defined by the *red-boxed area* in western Siberia in Fig. 3a

Table 3 Same as Table 1, except for western Siberia

Index	BL	LCC	ISHF
BL	1		
LCC	0.15	1	
ISHF	*0.56*	0.18	1

future (Meehl et al. 2007), we infer that the TPSC may play an increasingly significant role in shaping the Eurasian heat waves in next decades, particularly the SENA region.

It should be pointed out that by contrast to the SENA region (Fig. 10), LCC, ISHF and BL do not consistently exhibit an in-phase relationship with each other in western Siberia, only BL significantly correlated with ISHF (Fig. 11; Table 3). This indicates that the TPSC cannot trigger the above positive land–atmosphere feedback in western Siberia which is represented by the red-boxed area (50°–90°E, 60°–75°N) in Fig. 3a. Furthermore, the SGCM discrepancies in northern Europe (Figs. 3, 9) also imply that the TPSC anomaly cannot well interpret the circulation variations over this region. These results are consistent with the fact that the TPSC can explain only a small portion of the total variances of HWF over northern Eurasia (Fig. 2c).

Fig. 12 **a** Long-term mean (%) (*contours*) and standard deviations (%) (*color shadings*) of the northern Eurasian snow cover in JJA for the period 1967–2014. The snow cover averaged in the *purple-boxed area* (60°–180°E, 65°–80°N) is defined as a northern Eurasia snow cover index. **b** JJA HWF anomalies regressed against the northern Eurasia snow cover index (*contours*, in unit of day). The *shaded areas* exceed the 95 % confidence level based on the Student's-*t* test
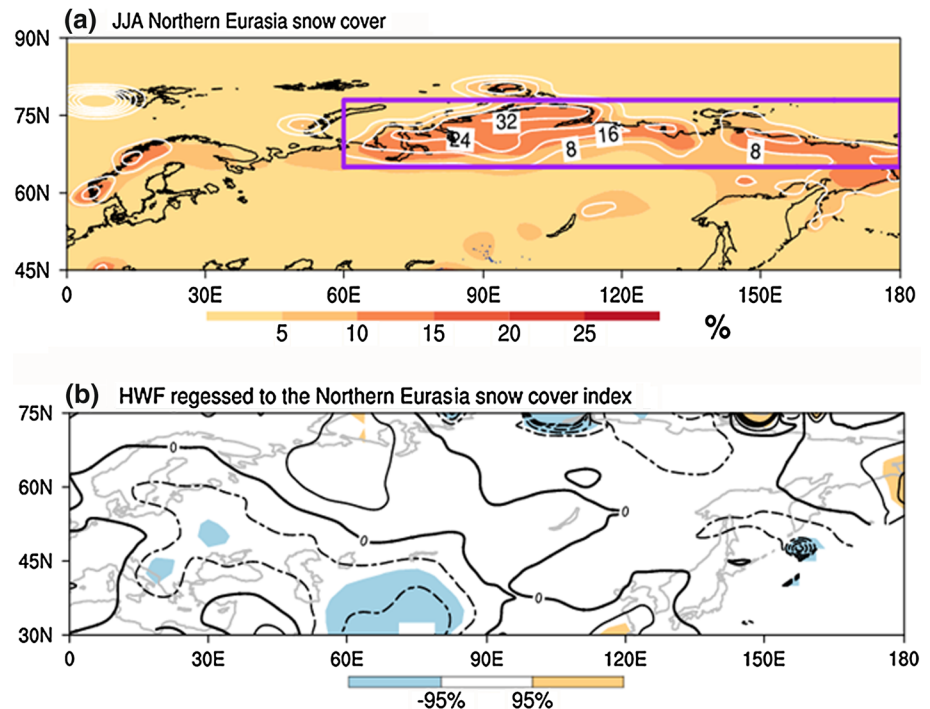
Although the TPSC was usually considered to be a portion of the Eurasian snow cover (Clark and Serreze 2000), it exhibits some unique features distinguished from the northern Eurasia snow cover (e.g., Wu and Zhang 1998; Zhang et al. 2004; Wang et al. 2008; Lin and Wu 2011). Figure 12a displays the climatology and standard deviation of the mid-high latitude Eurasian snow cover in summer for the period 1967–2014. Notable snow cover exists in northern Eurasia and exhibits significant year-to-year variability. If we define the snow cover anomaly averaged within the boxed domain (60°–180°E, 65°–80°N) as a northern Eurasia snow cover index, the correlation coefficient between the detrended TPSI and the northern Eurasian snow cover index (NESI) is 0.29 for the period 1967–2014. This indicates that the TPSC exhibits a certain degree of connection with the northern Eurasia snow cover. However, the HWF pattern regressed to the NESI does not resemble that to the TPSI (Fig. 12b and Fig. 2c). This indicates that the TPSC and the northern Eurasian snow cover may exert different effects on Eurasian heat waves. Due to the paper length limitation, the relative significance of the TPSC and the northern Eurasian snow cover on modulating the Eurasian heat waves will be examined in future work.

One major roadblock in performing analysis of climate impacts of the TPSC (or TP thermal effects) is the lack of access to high-quality and long-term climate data (Wu and Zhang 1998; Wang et al. 2008; Duan and Wu 2008, 2009). The gauge stations over the TP are quite sparse, particularly in the western TP. Satellite observation was not introduced into the meteorological monitoring (including snow cover monitoring) until late 1970s. Therefore, it is arduous to obtain unequivocal evidence of climate change by using the observational and statistical analysis alone. The combination with the use of numerical experiments may help to support the observational analysis.

In addition, Eurasian HWF may have other influential factors besides the TPSC. For instance, both the reduced TPSC and the increase of summer heat wave activities over Eurasia could be the result of large scale circulation change resulted from external forcing, such as increase of greenhouse gas concentrations (Meehl and Tebaldi 2004; Meehl et al. 2007, 2009). Nevertheless, the greenhouse effect dominated by a notable increasing trend can hardly interpret the interannual linkage between the TPSC and Eurasian HWF. Furthermore, natural factors, such as El Niño and the North Atlantic Oscillation, may also contribute to changes in the TPSC (e.g., Shaman and Tziperman 2005; Wu et al. 2009, 2012b). How to distinguish anthropogenic and natural variations in the TPSC variability remains as an outstanding issue and calls for further observational and numerical studies.

References

Alexander L (2010) Extreme heat rooted in dry soils. Nat Geosci 3:1–2

Barnett TP, Dümenil L, Schlese U, Roeckner E (1988) The effect of Eurasian snow cover on global climate. Science 239(4839):504–507

Barriopedro D, Fischer EM, Luterbacher J, Trigo RM, Garcia-Herrera RG (2011) The hot summer of 2010: redrawing the temperature record map of Europe. Science 332:220–224

Bretherton CS, Widmann M, Dymnikov VP, Wallace JM, Blade I (1999) Effective number of degrees of freedom of a spatial field. J Clim 12:1990–2009

Caesar J, Alexander L, Vose R (2006) Large-scale changes in observed daily maximum and minimum temperatures: creation and analysis of a new gridded dataset. J Geophys Res 111:D05101. doi:10.1029/2005JD006280

Clark MP, Serreze MC (2000) Effects of variations in East Asian snow cover on modulating atmospheric circulation over the North Pacific Ocean. J Clim 13:3700–3710

Compo GP, Whitaker JS, Sardeshmukh PD (2006) Feasibility of a 100 year reanalysis using only surface pressure data. Bull Am Meteorol Soc 87:175–190

Compo GP, Whitaker JS, Sardeshmukh PD, Matsui N, Allan RJ, Yin X, Gleason BE, Vose RS, Rutledge G, Bessemoulin P, Brönnimann S, Brunet M, Crouthamel RI, Grant AN, Groisman PY, Jones PD, Kruk M, Kruger AC, Marshall GJ, Maugeri M, Mok HY, Nordli Ø, Ross TF, Trigo RM, Wang XL, Woodruff SD, Worley SJ (2011) The twentieth century reanalysis project. Q J R Meteorol Soc 137:1–28

D'Ippoliti D, Michelozzi P, Marino C et al (2010) The impact of heat waves on mortality in 9 European cities: results from the Euro-HEAT project. Environ Health 9:37

Ding QH, Wang B (2005) Circumglobal teleconnection in the Northern Hemisphere summer. J Clim 18:3483–3505

Ding YH, Ren GY, Zhao ZC, Xu Y, Luo Y, Li QP, Zhang J (2007) Detection, causes and projection of climate change over China: an overview of recent progresses. Adv Atmos Sci 24(6):954–971

Duan AM, Wu GX (2008) Weakening trend in the atmospheric heat source over the Tibetan Plateau during recent decades. Part I: observations. J Clim 21:3149–3164

Duan AM, Wu GX (2009) Weakening trend in the atmospheric heat source over the Tibetan Plateau during recent decades. J Clim 22:4197–4212

Fischer EM, Schär C (2010) Consistent geographical patterns of changes in high-impact European heatwaves. Nat Geosci 3:398–403

Fischer EM, Seneviratne SI, Vidale PL, Lüthi D, Schär C (2007) Soil moisture–atmosphere interactions during the 2003 European summer heat wave. J Clim 20:5081–5099

Fletcher CG, Hardiman SC, Kushner PJ, Cohen J (2009) The dynamical response to snow cover perturbations in a large ensemble of atmospheric GCM integrations. J Clim 22:1208–1222

Fu CB (2003) Potential impacts of human-induced land cover change on East Asia monsoon. Glob Planet Change 37:219–229

Gong G, Entekhabi D, Cohen J (2002) A large-ensemble model study of the wintertime AO/NAO and the role of interannual snow perturbations. J Clim 15:3488–3499

Gong G, Entekhabi D, Cohen J (2003) Relative impacts of Siberian and North American snow anomalies on the winter Arctic Oscillation. Geophys Res Lett 30(16):1848. doi:10.1029/2003GL017749

Gong G, Entekhabi D, Cohen J, Robinson D (2004) Sensitivity of atmospheric response to modeled snow anomaly characteristics. J Geophys Res 109:D06107. doi:10.1029/2003JD004160

Hall NMJ (2000) A simple GCM based on dry dynamics and constant forcing. J Atmos Sci 57:1557–1572

Hall NMJ, Derome J (2000) Transients, nonlinearity, and eddy feedback in the remote response to El Niño. J Atmos Sci 57:3992–4007

Hirschi M, Seneviratne SI, Alexandrov V, Boberg F, Boroneant C, Christensen OB, Formayer H, Orlowsky B, Stepanek P (2010) Observational evidence for soil-moisture impact on hot extremes in southeastern Europe. Nat Geosci. doi:10.1038/NGEO1032

Lin H (2009) Global extratropical response to diabatic heating variability of the Asian summer monsoon. J Atmos Sci 66:2693–2713

Lin H, Wu ZW (2011) Contribution of the autumn Tibetan Plateau snow cover to seasonal prediction of North American winter temperature. J Clim 24:2801–2813

Lin H, Wu ZW (2012a) Contribution of Tibetan Plateau snow cover to the extreme winter conditions of 2009/10. Atmos Ocean 50(1):86–94

Lin H, Wu ZW (2012b) Indian summer monsoon influence on the climate in the North Atlantic-European region. Clim Dyn 39:303–311

Livezey RE, Chen WY (1983) Statistical field significance and its determination by Monte Carlo techniques. Mon Weather Rev 111:46–59

Luo HB, Yanai M (1984) The large-scale circulation and heat sources over the Tibetan Plateau and surrounding areas during the early summer of 1979. Part II: heat and moisture budgets. Mon Weather Rev 112:966–989

Meehl GA, Tebaldi C (2004) More intense, more frequent, and longer lasting heat waves in the 21st century. Science 305(5686):994–997

Meehl GA et al (2007) Global climate projections. In: Solomon S et al (eds) Climate change 2007: the physical science basis: fourth assessment report of the intergovernmental panel on climate change. Cambridge University Press, Cambridge

Meehl GA et al (2009) Decadal prediction. Bull Am Meteorol Soc 90:1467–1485

North GR, Bell TL, Cahalan RF, Moeng FJ (1982) Sampling errors in the estimation of empirical orthogonal functions. Mon Weather Rev 110:699–706

Perkins SE, Alexander LV (2013) On the measurement of heat waves. J Clim 26:4500–4517

Pu ZX, Xu L, Salomonson VV (2007) MODIS/Terra observed seasonal variations of snow cover over the Tibetan Plateau. Geophys Res Lett 34:L06706. doi:10.1029/2007GL029262

Qiu J (2014) Tibetan plateau gets wired up for monsoon prediction. Nature 514:16–17

Robinson DA, Frei A (2000) Seasonal variability of Northern Hemisphere snow extent using visible satellite data. Prof Geogr 51:307–314

Robinson DA, Dewey KF, Heim R (1993) Global snow cover monitoring: an update. Bull Am Meteorol Soc 74:1689–1696

Shaman J, Tziperman E (2005) The effect of ENSO on Tibetan Plateau snow depth: a stationary wave teleconnection mechanism and implications for the South Asian monsoons. J Clim 18:2067–2079

Sobolowski S, Gong G, Ting M (2010) Modeled climate state and dynamic responses to anomalous North American snow cover. J Clim 23:785–799

Sutton RT, Hodson DL (2005) Atlantic ocean forcing of North American and European summer climate. Science 309:115–118

Trenberth KE (1984) Some effects of finite sample size and persistence on meteorological statistics. Part I: auto-correlations. Mon Weather Rev 112:2359–2368

Trenberth KE, Jones PD, Ambenje P, Bojariu R, Easterling D, Klein Tank A, Parker D, Rahimzadeh F, Renwick JA, Rusticucci M, Soden B, Zhai P (2007) Observations: surface and atmospheric

climate change. In: Solomon S, Qin D, Manning M, Chen Z, Marquis M, Averyt KB, Tignor M, Miller HL (eds) Climate change 2007: the physical science basis. Contribution of working group 1 to the fourth assessment report of the intergovernmental panel on climate change. Cambridge University Press, Cambridge

Wang B, Ding Q (2006) Changes in global monsoon precipitation over the past 56 years. Geophys Res Lett 33:L06711. doi:10.1029/2005GL025347

Wang B, Bao Q, Hoskins B, Wu GX, Liu YM (2008) Tibetan Plateau warming and precipitation change in East Asia. Geophys Res Lett 35:L14702. doi:10.1029/2008GL034330

Whitaker JS, Compo GP, Wei X, Hamill TM (2004) Reanalysis without radiosondes using ensemble data assimilation. Mon Weather Rev 132:1190–1200

Wu GX, Zhang YS (1998) Tibetan Plateau forcing and the timing of the monsoon onset over South Asia and the South China Sea. Mon Weather Rev 126:913–927

Wu ZW, Wang B, Li JP, Jin FF (2009) An empirical seasonal prediction model of the East Asian summer monsoon using ENSO and NAO. J Geophys Res 114:D18120. doi:10.1029/2009JD011733

Wu ZW, Jiang ZH, Li JP, Zhong SS, Wang LJ (2012a) Possible association of the western Tibetan Plateau snow cover with the decadal to interdecadal variations of Northern China heatwave frequency. Clim Dyn 39:2393–2402

Wu ZW, Li JP, Jiang ZH, Ma TT (2012b) Modulation of the Tibetan Plateau snow cover on the ENSO teleconnections: from the East Asian summer monsoon perspective. J Clim 25:2481–2489

Wu ZW, Li JP, Jiang ZH, He JH, Zhu XY (2012c) Possible effects of the North Atlantic Oscillation on the strengthening relationship between the East Asian summer monsoon and ENSO. Int J Climatol 32:794–800

Wu ZW, Lin H, Li JP, Jiang ZH, Ma TT (2012d) Heat wave frequency variability over North America: two distinct leading modes. J Geophys Res 117:D02102. doi:10.1029/2011JD016908

Zhai PM, Sun AJ, Ren FM, Liu XN, Gao B, Zhang Q (1999) Changes of climate extremes in China. Clim Change 42:203–218

Zhang YS, Li T, Wang B (2004) Decadal change of snow depth over the Tibetan Plateau in spring: the associated circulation and its relationship to the East Asian summer monsoon rainfall. J Clim 17:2780–2793

Zhong SS, Wu ZW, He JH (2013) Comparisons of the thermal effects of the Tibetan Plateau with NCEP-I and ERA-40 reanalysis data. Atmos Ocean 51(1):75–87